Gadolinium-Conjugated Folate–Poly(ethylene Glycol)–Polyamidoamine Dendrimer–Carboxyl Nanoparticles as Potential Tumor-Targeted, Circulation-Prolonged Macromolecular Magnetic Resonance Imaging Contrast Agents. II

Wei-Lu Zhang,[1,2] Na Li,[2] Jin Huang,[2] Shu-Fang Luo,[2] Ming-Xia Fan,[3] Shi-Yuan Liu,[4] Ben Muir,[5] Jia-Hui Yu[2]

[1]*Department of Applied Chemistry, College of Chemistry and Materials Science, Wenzhou University, Wenzhou 325027, Zhejiang Province, People's Republic of China*
[2]*Institutes for Advanced Interdisciplinary Research, East China Normal University, Shanghai 200062, People's Republic of China*
[3]*Shanghai Key Laboratory of Functional Magnetic Resonance Imaging, East China Normal University, Shanghai 200062, People's Republic of China*
[4]*Department of Diagnostic Imaging, Changzheng Hospital, Shanghai 200003, People's Republic of China*
[5]*The Commonwealth Scientific and Industrial Research Organisation, Bayview Ave, Bag 10, Clayton South, Melbourne, Victoria 3169, Australia*

Received 19 August 2010; accepted 1 December 2010
DOI 10.1002/app.33841
Published online 7 April 2011 in Wiley Online Library (wileyonlinelibrary.com).

ABSTRACT: A new macromolecular gadolinium-based magnetic resonance imaging (MRI) contrast agent, folic acid (FA)–poly(ethylene glycol) (PEG)–polyamidoamine dendrimer (PAMAM)–Gd, was synthesized with a core of PAMAM, which was modified with conjugates of FA and PEG and then chelated by gadolinium ions. The final products, with FA as the targeting moiety, were evaluated for their tumor-targeting MRI contrast-agent potential. The concentration detection limits *in vitro*; contrast-enhanced MRI in the heart, kidney, and liver of mice; and metabolism of FA–PEG–PAMAM–Gd were measured by a Siemens Tim Trio human MRI scanner at 3 T. Transmission electron microscopy was used to determine the targeting of FA–PEG–PAMAM–Gd to human epidermoid carcinomas cell lines (KB) or murine aneuploid fibrosarcoma cell lines (L929). The toxicity was also assayed to evaluate the biocompatibility of this contrast agent. The minimum detectable concentration of FA–PEG_{4K}–PAMAM–Gd (where the subscript 4K indicates a molecular weight of 4000 Da) was 15-fold lower than that of the commercially available contrast agent gadopentetate dimeglumine. The MRI images displayed a gradual persistent signal enhancement on tumors, and millimeter-sized ($\sim$ 3 mm) tumors were well visualized with FA–PEG_{4K}–PAMAM–Gd. In conclusion, the dendritic complexes were well suited for use as an FA-mediated targeting contrast agent for early diagnosis of tumors in mice. The dendritic contrast agents displayed lower concentration detection limits, which suggests their future use in molecular imaging. © 2011 Wiley Periodicals, Inc. J Appl Polym Sci 121: 3175–3184, 2011

Key words: biological applications of polymers; dendrimers; drug delivery systems

INTRODUCTION

Magnetic resonance imaging (MRI) provides not only an anatomical resolution with good delineation of lesions but also functional information in a noninvasive and real-time monitoring manner.[1] In addition, MRI provides much greater contrast between the different soft tissues of the body than computed tomography does; this makes it especially useful in neurological, musculoskeletal, cardiovascular, and oncological imaging.[2] Diseases, including mental disorders and cancer, which often result in bad prognoses when there is a lack of early diagnosis, can be monitored via MRI.

However, MRI is much less sensitive than other imaging methods when used to monitor small tissue

Correspondence to: W.-L. Zhang (zwlcxq@hotmail.com) or J.-H. Yu (jhyu@sist.ecnu.edu.cn).

Contract grant sponsor: Wenzhou City Commission for Society Development Project; contract grant number: S20090007.
Contract grant sponsor: Shanghai Municipality Commission for Nongovernmental International Corp. Project; contract grant number: 09540709000.
Contract grant sponsor: Shanghai Municipality Commission for Special Project of Nanometer Science and Technology; contract grant numbers: 0952nm05300, 0852nm03700.
Contract grant sponsor: Shanghai Municipality Commission for Governmental International Corp. Project; contract grant number: 10410710000.

lesions, molecular activities, or cellular activities.[3] As such, in the past decade, contrast agents have been used to resolve these problems. Today, about 30–35% of all MRI investigations are contrast-agent-enhanced studies. Gadolinium chelators are frequently used as MRI contrast agents because of their high magnetic moment, asymmetric electronic ground state, and potential for increased MRI intensity.[4,5]

Dendrimers have defined structures and a large number of available surface groups; this has led to their use in many fields, especially as substrates for the attachment of large numbers of chelating agents.[6–8] Dendrimers are also excellent macromolecular scaffolds for the attachment of multiple Gd(III) complexes.[6] Several studies have shown that dendrimers are excellent macromolecules for the synthesis of MRI contrast agents.[9–11] In particular, polyamidoamine dendrimers (PAMAM) are often used for vascular and molecular imaging because of their prolonged retention in the circulation and their enhanced relaxitivities.[6,12] However, toxicity problems limit their biomedical potential. Conjugation with poly(ethylene glycol) (PEG) chains has been considered a method of reducing the toxicity and increasing the biocompatibility of dendrimers because PEG is nontoxic and nonimmunogenic and has favorable pharmacokinetics and tissue distribution.[13,14] The half-maximal inhibitory concentration values of polyethylene glycolated (PEGylated) dendrimers are 12- to 105-fold higher than those of PAMAM dendrimers.[15]

Recently, surface-conjugated PAMAM dendrimers with targeting ligands have received much attention because these ligands have been found to have a number of benefits, including an improved accuracy of diagnoses, a decrease in toxicity, and a prolonged circulation time.[16] Additionally, the high targeting efficiency of these compounds *in vivo* may decrease medication dosages and improve contrast effects.[17] Active targeting, especially, was developed to improve specific accumulation in tumor cells via receptor-mediated endocytosis. One of these receptors is folate receptor (FR), which is a valuable therapeutic target that highly expressed in a variety of cancers, including ovarian carcinomas, endometrial cancer, kidney cancer, lung cancer, mesothelioma, breast cancer, brain cancer and myeloid leukemia[18,19] The fact that many cancers overexpress FRs, whereas most normal tissues express low-to-negligible levels, makes it exploitable in the clinical application of folic acid (FA)-targeted imaging and therapeutic agents.[20] For example, a dendrimer-based Gd chelate has been applied for the detection of FR-positive tumors.[21–23] However, this chelate is synthesized with a low-molecular chelator and results in the addition of synthesis steps.

From the aforementioned considerations for an ideal macromolecular MRI contrast agent, a facile and inexpensive approach to the development of a potential tumor-targeted and circulation-prolonged macromolecular MRI contrast agent without the use of low-molecular gadolinium ligands is described in this article. FA–PEG–PAMAM–Gd macromolecular MRI contrast agents were prepared and characterized by ^{1}H-NMR and Fourier transform infrared (FTIR) spectroscopy. The toxicity, MRI *in vivo* and *in vitro*, and tumor-targeted profile of FA–PEG–PAMAM–Gd were also tested. The new FR-based gadolinium chelates are expected to improve the sensitivity and specificity of MRI for early clinical diagnosis of cancer.

EXPERIMENTAL

Materials

A generation-3 PAMAM with 32 terminal carboxyl groups (PAMAM–COOH) and a molecular weight of 6909 Da, FA, PEG [weight average molecular weight (M_w) = 4000 Da], and methoxy poly(ethylene glycol) (mPEG, M_w = 4000 Da) were purchased from Sigma-Aldrich (Shanghai, China). α-Methoxy-ω-amino–poly(ethylene glycol) ($mPEG_{4K}$–NH_2, where the subscript 4K indicates a molecular weight of 4000 Da) and PEG–bisamines (NH_2–PEG_{4K}–NH_2) were synthesized according to the literature.[24] Dimethyl sulfoxide was distilled before use. A stock $GdCl_3$ solution was prepared by the dissolution of $GdCl_3 \cdot 6H_2O$ in deionized water.

Propidium iodide (> 95%), acridine orange (dye content = 90%), trypsin (1 : 250) powder, fetal bovine serum (FBS), streptomycin/ampicillin solution, RPMI-1640, and F-12K cell culture medium were purchased from (Gibco, Michigan).

Animal tumor model

Male athymic nude mice (2 weeks old) were maintained and cared for under a protocol approved by our institute. The mice were maintained in hygienic and ventilated cages and fed a special low-FA diet ([casein] = 100 g/kg, [soya protein] = 100 g/kg, [soyabean] = 70 g/kg, [cellulose] = 47.5 g/kg, [cornstarch] = 170 g/kg, [sucrose] = 450 g/kg, [FA-free vitamin mix] = 12.68 g/kg, [choline] =1.5 g/kg, [butyleret hydroxytoluen] = 0.014 g/kg, [L-cystine] = 3.3 g/kg) from 1 week before tumor inoculation until the mice were sacrificed for *in vivo* performance determination.[25]

KB cell lines (human epidermoid carcinomas) and L929 (murine aneuploid fibrosarcoma cell lines) (Cell Bank of Chinese Academy of Sciences, Shanghai, China) were grown continuously at 37°C and 5% CO_2 in FA-free RPMI 1640 medium supplemented with 10% inactivated FBS, streptomycin at

100 U/mL penicillin, and 100 μg/mL streptomycin. Aliquots of 0.2 mL of a phosphate buffered saline mixture containing about 1×10^6 KB cells were implanted subcutaneously in the right axilla of the mice when they weighed about 25 g. Tumors were normally visible 1 week after injection; a tumor 0.7–1.0 cm in diameter was generated after about 30 days of growth.

Synthesis of FA–PEG–PAMAM–Gd

The synthesis of FA–PEG–PAMAM–COOH was performed according to a previous method.[26] Briefly, the γ-carboxyl group of FA was reacted with one of the amino groups of PEG–bisamine (NH_2–PEG_{4K}–NH_2, $M_w = 4000$ Da) at a molar ratio of 1 : 1 in dimethyl sulfoxide to obtain the conjugate of FA–PEG_{4K}–NH_2. The solution of FA–PEG_{4K}–NH_2 was then added dropwise to a solution of PAMAM–COOH (32 carboxyl groups) at a molar ratio of 8 : 1. The number of FA–PEG moieties conjugated per mole of PAMAM was estimated with ^{1}H-NMR and FTIR spectroscopy.

The final product of gadolinium-based FA–PEG–PAMAM–Gd was prepared according to a typical procedure.[27] FA–PEG_{4K}–PAMAM–COOH dissolved in 5 mL of double-distilled water was added dropwise to a solution of $GdCl_3 \cdot 6H_2O$. The mixture was stirred for 24 h under no-light conditions. FA–PEG_{4K}–PAMAM–Gd complexes were purified with gel chromatography on a Sephadex-G25 column (Pharmacia, Stockholm, Sweden) to remove free Gd^{3+}. The mass percentage content of Gd(III) in FA–PEG_{4K}–PAMAM–Gd was measured by inductively coupled plasma–atomic emission spectrometry (Thermo Electron IRIS Intrepid II XSP, Thermo Electron, Massachusetts). The longitudinal relaxivity (r_1) of FA–PEG_{4K}–PAMAM–Gd was 64.88 mM^{-1} s^{-1} and was based on the study of the relaxivity of FA–PEG_{4K}–PAMAM–Gd as a function of the concentration of Gd.

In vitro MRI

Magnetic resonance (MR) measurements were performed with a circular surface coil (inner diameter = 18 cm). Solutions of the prepared samples and the commercially available contrast agent gadopentetate dimeglumine (DTPA–Gd) in deionized water were prepared with Gd(III) concentrations ranging from 1.25×10^{-4} to 2.50×10^{-2} mmol/L in vials with an inner diameter of 5 mm. MR images were produced with an inversion recovery sequence at 3.0 T with a repetition time (TR) of 5000 ms, an echo time (TE) of 7.6 ms, and a number of averages of 2. The average signal intensity was measured in circular regions of interest in the central section of each vial. The relative signal change, defined as $(S - S_0)/S_0$, where S represents the MRI signal at a specified concentration and S_0 represents the MRI signal at zero concentration, was then calculated.

In vivo MRI

The white mice (~ 30 g, Number (N) = 4) were anesthetized by the intraperitoneal administration of 60 mg of pentobarbital sodium (Sigma-Aldrich, Shanghai, China) per kilogram of body weight and then positioned and stabilized in the scanner by a wrist coil. The samples of DTPA–Gd were injected intravenously through a tail vein with the same dose of 0.1 mmol of Gd(III)/kg body weight. Warm water bags were placed near the mice to keep the local temperature in the MRI unit bore near 28°C. The mice were scanned before and after the administration of any contrast agents. MR images were collected multiple times. For T1-weighted imaging at 3 T, a spin-echo sequence was used with parameters of TE/TR = 12 ms/550 ms, field of view = 60×60 mm^2, slice number = 15, voxel size = $0.1875 \times 0.1875 \times 2$ mm^3, and flip angle = 120°. MR images were then analyzed with Syngo fastView software (Siemens, Munich, Germany). The MR signal intensity in several organs was ascertained by the average intensity in the defined regions of interest or voxels within the organs. After MRI, the mice were sacrificed via cervical dislocation while they were under anesthesia.

Tumor targeting evaluation

BALB/c nude mice (average body weight = 25.0 ± 2.0 g) were used for *in vivo* targeting studies. Nude mice with KB tumors were anesthetized by the intraperitoneal administration of 60 mg of pentobarbital sodium (Sigma) per kilogram of body weight and then placed in a surface coil (inner diameter = 5 cm). Each animal was kept warm during the MRI scan. FA–PEG_{4K}–PAMAM–Gd, at a concentration of 6.2 mg/mL, was injected intravenously through a tail vein at a dose of 0.05 mmol Gd(III)/kg of body weight. DTPA–Gd (0.16 mmol/kg, 80 μL) was used as a control. Serial MR images were acquired 5 min after the injection at 3 T. A two-dimensional (2D) T1-weighted spin-echo sequence was used to acquire tumor images. The spin-echo sequence parameters were as follows: field of view = 60 mm × 60 mm^2, TR/TE = 550 ms/12 ms, voxel size = $0.1875 \times 0.1875 \times 2$ mm^3, and flip angle = 120°. MR images were analyzed with Syngo fastView software. The regions of interest in each mouse were set at the tumor rim and tumor interstitium in the spin-echo images. The relative intensities were calculated as the ratios of the signal intensities after injection to

the signal intensities before injection observed in corresponding regions of interest.

Molecular targeting measurement

The molecular targeting of FA–PEG_{4K}–PAMAM–Gd was measured by transmission electron microscopy (TEM). Aliquots of 1×10^6 KB or L929 cell lines were cultured with FA-free RMPI 1640 culture medium in Petri dish for 24 h at 37°C in a 5% CO_2-containing incubator. The culture medium was replaced by RMPI 1640 fresh culture medium (10 mL) with 10% FBS. A 1-mg sample containing 1% penicillin–streptomycin of FA–PEG_{4K}–PAMAM–Gd or PEG_{4K}–PAMAM–Gd (as control) was added and cultured for 24 h. KB or L929 cell lines incubated with the samples were washed three times with phosphate buffered saline solution, digested by 0.1% trypsin, and fixed with 2% glutaraldehyde for 3 h. In addition, the cells were postfixed in 1% osmium tetraoxide for 30 min, then washed, and dehydrated in graded concentrations of ethanol (25, 50, 70, and 100%) and propylene oxide. The cell samples were embedded in Epon and then thin-sectioned. These thin sections of approximately 50 nm were cut, collected on copper grids, and stained with 4% lead citrate. Subsequently, the sections were measured by JEM-2100 TEM (Hitachi, Tokyo, Japan) and photographed.

In vivo toxicity evaluation

The mice were randomly divided into three groups: groups A, B, and C, with six cases in each group. The three groups of mice were then tested with different methods. For group A (as a control), the mice were anesthetized by the intraperitoneal administration of 60 mg of pentobarbital sodium (0.02 g/mL, Sigma) per kilogram of body weight. Their organs, specifically the heart, liver, kidney, lungs, and tumor, were then surgically removed and washed with a normal saline solution. These organs were fixed in 4% paraformaldehyde for 3 h, embedded in Epon, serially sectioned (4 μm), and stained with hematoxylin–eosin. The sections were observed with an Olympus IX71 microscope equipped with a DP71 charged coupling device camera (Olympus, Tokyo, Japan). For groups B and C, the process of operation was the same as that of group A, except that FA–PEG_{4K}–PAMAM–Gd (6.2 mg/mL) was intravenously injected once every 3 h for 3 days through a tail vein at a dose of 0.1 mmol/kg of body weight for group B and once every 2 days for 3 months (group C) to evaluate the toxicity of the drug.

Statistical analysis

Data were expressed as the means with 95% confidence intervals. The statistical analyses of MRI signal intensity were performed with a one-factor analysis of variance (Syngo fastView software, version 1.0, Siemens AG Medical Solutions, Department SW, Erlangen). *P* values of less than 0.05 were considered to be statistically significant. All statistical tests were two-sided.

RESULTS AND DISCUSSION

Synthesis and characterization of FA–PEG–PAMAM–Gd

The macromolecular gadolinium-based chelator FA–PEG_{4K}–PAMAM–COOH was synthesized through the coupling reaction of carboxylic groups in PAMAM–COOH and amino groups in FA–PEG_{4K}–NH_2. FA was used as a target group and conjugated with PAMAM with a spacer of PEG because high-affinity FR binding was retained even when FA was covalently linked to a foreign molecule via its γ-carboxyl group.[28] To improve the chelating ability and content of gadolinium in the resulting macromolecular MRI contrast agent, it was a key issue to synthesize the macromolecular MRI ligands with enough

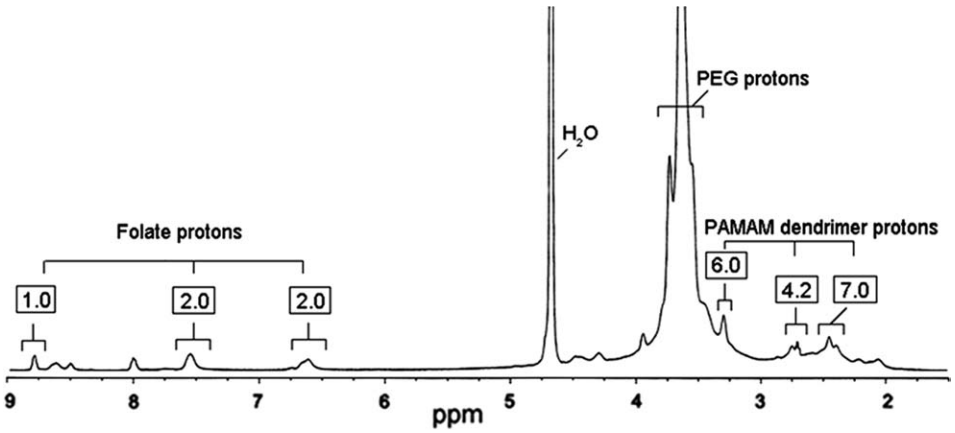

Figure 1 ^{1}H-NMR spectrum of FA–PEG_{4K}–PAMAM–COOH in D_2O.

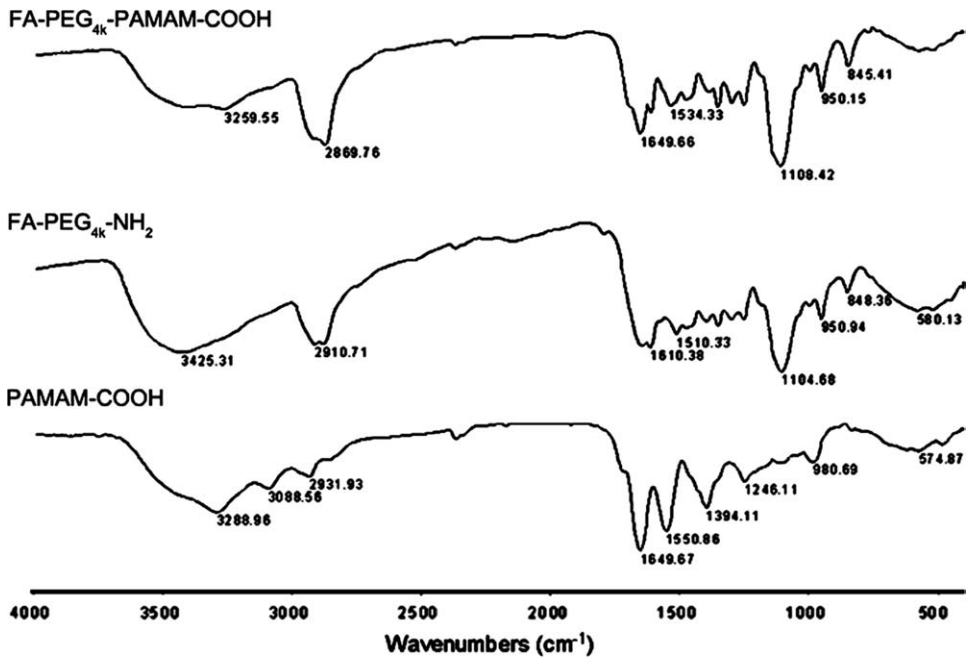

Figure 2 FTIR spectra of FA–PEG_{4K}–PAMAM–COOH, FA–PEG_{4K}–NH_2, and PAMAM–COOH.

chelating groups. Thus, the feed molar ratio of FA–PEG_{4K}–NH_2 to PAMAM–COOH was controlled at approximately 8 : 1. Structural characterization with ^{1}H-NMR and IR spectroscopy showed the perfect modification of FA–PEG_{4K}–NH_2 to the PAMAM–COOH dendrimer. Representative ^{1}H-NMR of purified FA–PEG_{4K}–PAMAM–COOH is shown in Figure 1. The aromatic FA proton peaks were observed at 6.65, 7.59, and 8.78 ppm, along with PEG protons at 3.47–3.75 ppm (the chemical-shift values measured with respect to tetramethylsilane at $\delta = 0$). The multiple proton peaks from PAMAM–COOH were found between 2.37 and 3.47 ppm. From the integral ratio of the FA proton at 8.78 ppm to the multiplets of PAMAM–COOH proton at 3.22 ppm, approximately six FA–PEG moieties were found to attach to each molecule of PAMAM–COOH. In other words, there were 25 free carboxylic groups remaining in each FA–PEG_{4K}–PAMAM–COOH molecule; these could be used to complex with gadolinium ions.

In the FTIR spectra (Fig. 2), the —NH— peaks shifted from 3425.31 cm^{-1} (FA–PEG_{4K}–NH_2) to 3259.55 cm^{-1} for FA–PEG–PAMAM conjugates, along with the characteristic PEG peaks of FA–PEG_{4K}–NH_2 at 1104.68 cm^{-1} shifting to 1108.42 cm^{-1}. These measurements confirmed the conjugation.

The polydispersity index (PDI) of FA–PEG–PAMAM–Gd measured by dynamic light scattering was 0.56, which was larger than that of the FA–PEG–PAMAM–COOH ligands. The results were mainly contributed to the conjugation of several

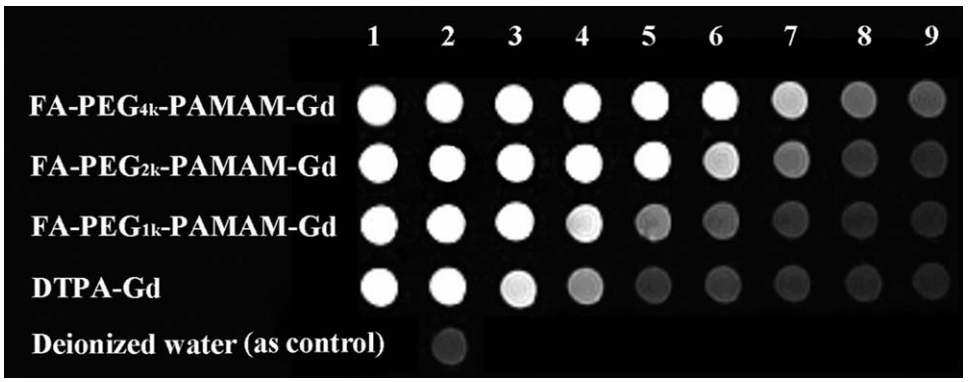

Figure 3 Comparison of *in vitro* T1-weighted MR images produced with an inversion recovery sequence at 3 T: FA–PEG_{4K}–PAMAM–Gd, FA–PEG_{2k}–PAMAM–Gd, FA–PEG_{1k}–PAMAM–Gd, DTPA–Gd, and deionized water (as a control). The Gd concentrations were (1) 2.50×10^{-2}, (2) 1.87×10^{-2}, (3) 1.25×10^{-2}, (4) 6.23×10^{-3}, (5) 2.50×10^{-3}, (6) 1.25×10^{-3}, (7) 6.23×10^{-4}, (8) 2.5×10^{-4}, and (9) 1.25×10^{-4} mmol/L, respectively.

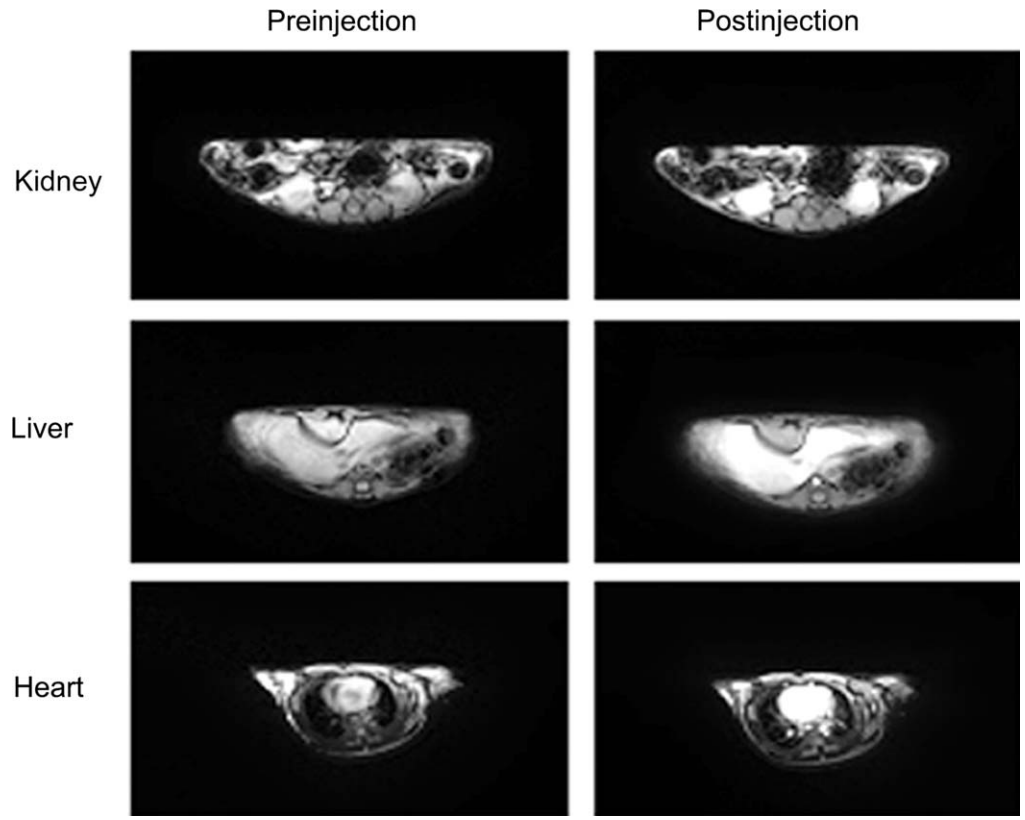

Figure 4 *In vivo* MRI contrast enhancement of the kidney, liver, and heart of mice preinjection (left) and 5-min postinjection (right) of FA–PEG_{4K}–PAMAM–Gd through the tail vein.

ligands with a gadolinium ion during the preparation. The increase in PDI significantly prolonged blood circulation and, consequently, increased the risk of cumulative toxicity *in vivo*.

In vitro MRI

The MRI signal intensity of FA–PEG–PAMAM–Gd complexes decreased by various degrees in T1-weighted imaging, depending on the Gd concentration in deionized water. The *in vitro* T1-weighted MR measurements showed that higher molecular weights of FA–PEG_{4K}–PAMAM–Gd and FA–PEG_{2k}–PAMAM–Gd gave the best signal enhancements at low concentrations (Fig. 3). The lower molecular weight contrast agents DTPA–Gd and FA–PEG_{1k}–PAMAM–Gd gave the best visual signal enhancement at higher concentrations. The signal intensity value of FA–PEG_{4K}–PAMAM–Gd at 1.25×10^{-3} mmol/L (1450 ± 38) was similar to that of DTPA–Gd at 1.87×10^{-2} mmol/L (1454 ± 54). These results show that the prepared samples of FA–PEG_{4K}–PAMAM–Gd had better contrast imaging at a lower concentration than that exhibited by DTPA–Gd, which in turn, meant that much lower dosages of FA–PEG_{4K}–PAMAM–Gd could be used to obtain the same MR images than the DTPA–Gd concentration required in clinical applications.

The r_1 of FA–PEG–PAMAM–Gd showed a tendency to increase with increasing molecular weight of PEG. The results contributed to the higher molecular weight of FA–PEG–PAMAM–Gd, which resulted in a longer rotational correlation lifetime of Gd, along with an increased r_1. The finding that the highest molecular weight MRI contrast agent of FA–PEG_{4K}–

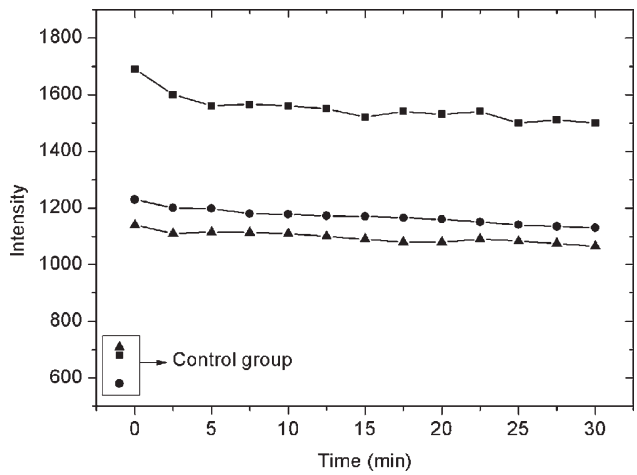

Figure 5 *In vivo* biodistribution of FA–PEG_{4K}–PAMAM–Gd: the MRI signal intensity changes in the kidney (●), liver (▲) and heart (■) as a function of time (the signal before 0 as a control).

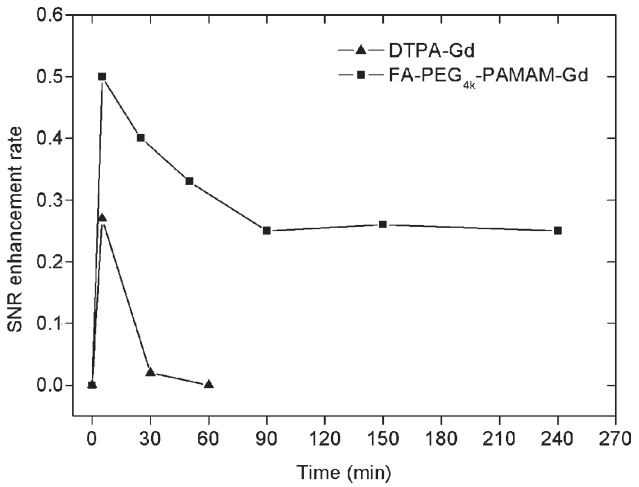

Figure 6 The SNR enhancement rate changed in the tumor as a function of time after injection of (■) FA–PEG_{4K}–PAMAM–Gd and (▲) DTPA–Gd (as a control), respectively.

PAMAM–Gd gave the lowest detection limit could make it potentially the best candidate for further molecular imaging purposes.

In vivo MRI

The effect of MRI contrast enhancement of the contrast agent was tested in mice. FA–PEG_{4K}–PAMAM–Gd was administered at a dosage of 0.1 mmol of Gd^{3+}/kg of body weight. A comparison of the precontrast and postcontrast T1-weighted spin-echo images of the kidney, liver, and heart is shown in Figure 4. These MR images were measured at 3.0 T at the same time point. As supplementary data to Figure 4, a time-dependent change-of-contrast enhancement over a period of 30 min is shown in Figure 5. The data before 0 indicates the preinjection control. The distribution of the contrast enhancement at different organs was shown by a quantitative analysis of signal intensity data and the greatest enhancement was observed at heart.

As shown in Figure 5, no significant change in the signal intensity was observed during the time period of observation. Contrast enhancement by FA–PEG_{4K}–PAMAM–Gd was sustained over 0–30 min in multiple organs; this indicated a much longer tissue retention time for FA–PEG_{4K}–PAMAM–Gd than for DTPA–Gd. In contrast to the short blood circulation time of DTPA–Gd, FA–PEG_{4K}–PAMAM–Gd

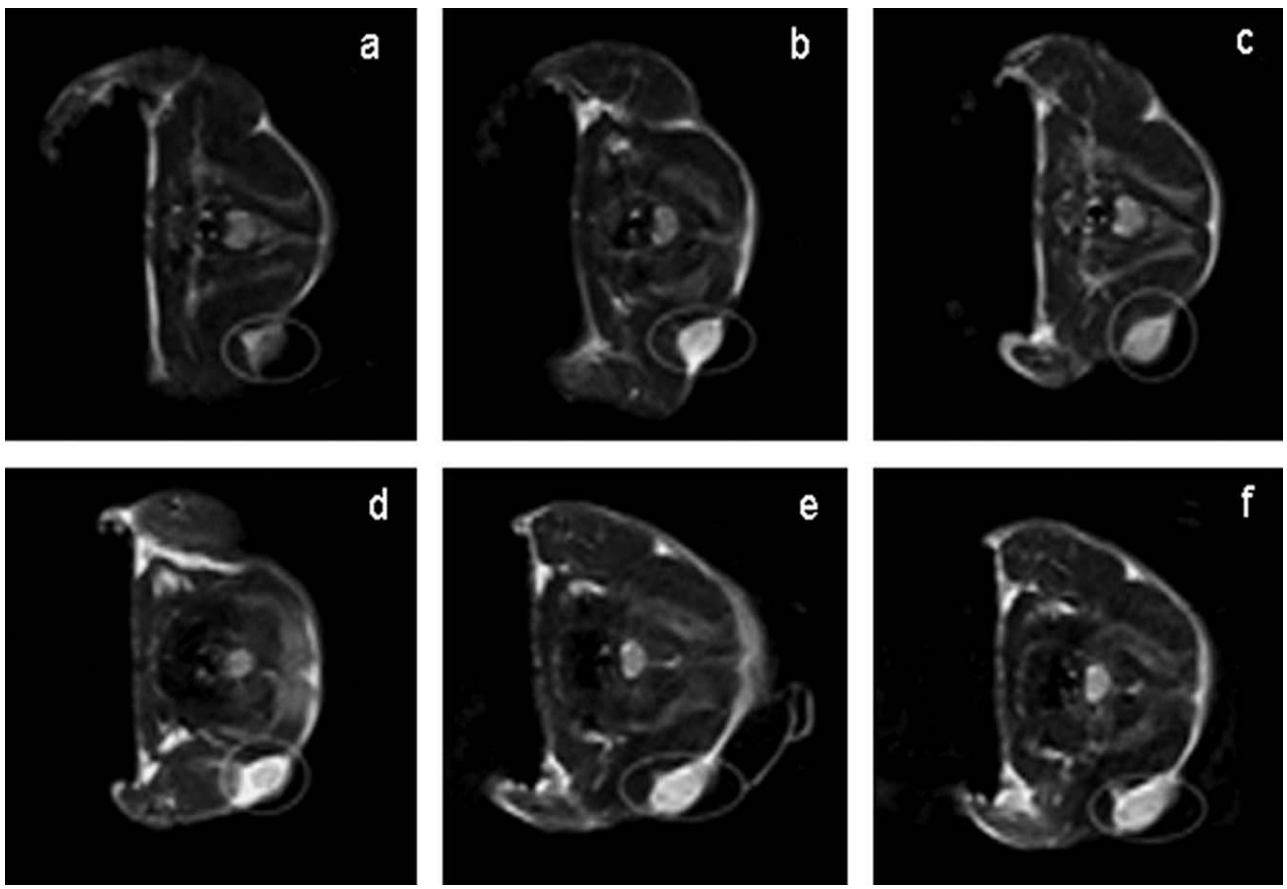

Figure 7 T1-weighted MRI images in tumors of mice at various time points before and after injection of: (a) pre-injection, (b) DTPA–Gd after 5 min, (c) mPEG–PAMAM–Gd after 5 min, (d) FA–PEG_{4K}–PAMAM–Gd after 5 min, (e) FA–PEG_{4K}–PAMAM–Gd after 25 min, and (f) FA–PEG_{4K}–PAMAM–Gd after 90 min.

exhibited a prolonged blood circulation time; it remained at high concentrations in the blood stream for longer periods of time with little background tissue enhancement. This is an important property for the imaging of clinical events that require prolonged periods of time. These results suggest that FA–PEG_{4K}–PAMAM–Gd is a good candidate as a blood-pool contrast agent.

Tumor targeting evaluation

In this study, MRI was used to study the distribution and metabolism of the prepared contrast agent of FA–PEG_{4K}–PAMAM–Gd in mice bearing tumors. Compared with the conventional method of radioactive isotope labeling, metabolism evaluation by MRI resulted in a decrease of radiation pollution. The plot of the signal-to-noise ratio (SNR) enhancement rate versus time is shown in Figure 6. The SNR enhancement rate peaked at 5 min after injection for both FA–PEG_{4K}–PAMAM–Gd and DTPA–Gd (as a control). FA–PEG_{4K}–PAMAM–Gd then decreased to a constant level for after 90 min. DTPA–Gd, on the other hand, disappeared after 30 min. At all observation points, significantly higher SNR enhancement rates were detected in tumor tissues targeted by FA–PEG_{4K}–PAMAM–Gd compared to DTPA–Gd. The analysis of SNR with time indicated that FA–PEG_{4K}–PAMAM–Gd accumulated in the tumor tissue at higher concentration levels; this also demonstrated the targeting properties of this contrast agent.

The targeting properties of FA–PEG_{4K}–PAMAM–Gd were proven by the MRI of the mice bearing tumors (Fig. 7). Figure 7(d) (after injection of FA–PEG_{4K}–PAMAM–Gd) shows the good delineation of the tumor tissue in MRI at an early time point (5 min after injection). The best effects were observed after the injection of FA–PEG_{4K}–PAMAM–Gd, in contrast to preinjection [Fig. 7(a)], with TDPA–Gd [Fig. 7(b)] and, especially, with mPEG–PAMAM–Gd [Fig. 7(c)], which was synthesized from mPEG–NH_2 and PAMAM–COOH, according to the same method used for FA–PEG–PAMAM–COOH. FA–PEG_{4K}–PAMAM–Gd induced a slight-to-moderate signal increase in tumors 25 min after injection [Fig. 7(e)] and 90 min after injection [Fig. 7(f)]. mPEG–PAMAM–Gd was less effective and showed only a slight delineation (or no delineation) of the tumor tissue; this could have contributed to the absence of FA. These results, along with more than 240 min distributions in the tumor tissue, showed that FA–PEG_{4K}–PAMAM–Gd could act as a macromolecular diagnostic contrast agent with its FR targeting properties. The fact that FA–PEG_{4K}–PAMAM–Gd could clearly show tumors 3 mm in size implied that it could be used for tumor angiogenesis imaging.[29]

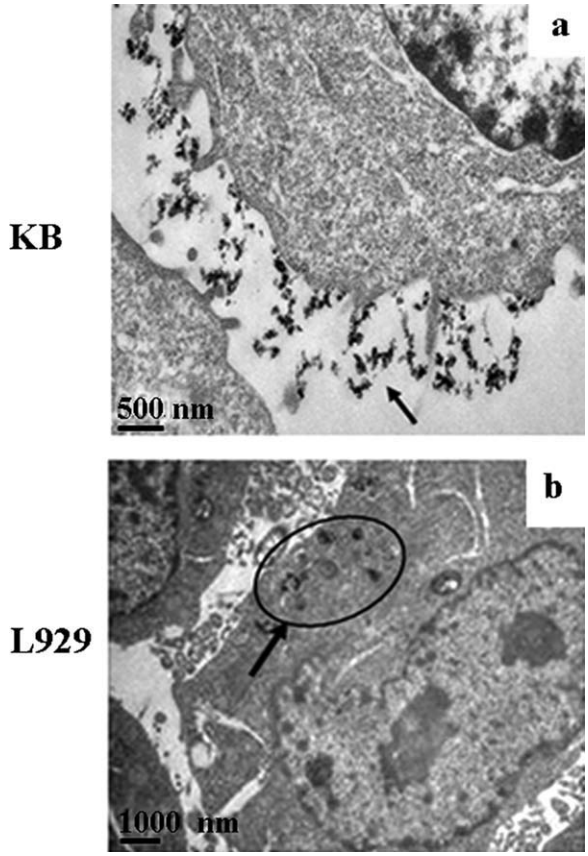

Figure 8 Sections with lead citrate stains displaying a high affinity of FA–PEG_{4K}–PAMAM–Gd to the (a) KB and (b) L929 cancer cells by TEM. The FA–PEG_{4K}–PAMAM–Gd contrast agents showed dark, positive targeting for FR (arrows).

Molecular targeting evaluation

The cancer cell lines KB were targeted by FA–PEG_{4K}–PAMAM–Gd to evaluate whether or not FA–PEG_{4K}–PAMAM–Gd selectively bonded to the selected cancer cells and whether or not this polymeric complex exhibited a higher targeting efficiency. The cells were observed with TEM to analyze the amount of the complex targeted in the cells. The FA–PEG_{4K}–PAMAM–Gd observed on the surface of KB cell lines [Fig. 8(a)] after 3 h of culturing indicated that FA–PEG_{4K}–PAMAM–Gd was a highly specific and selective contrast agent because of its binding affinity with the tumor cells. It is well-known that FA has a specific affinity for FR that is selectively expressed in some tumor cells and their neoangiogenic tissue. The significant targeting efficiency of FA–PEG_{4K}–PAMAM–Gd to KB was attributed to the FA moiety conjugating with FA–PEG_{4K}–PAMAM–Gd and FR in KB.

The targeting properties of FA–PEG_{4K}–PAMAM–Gd were also tested in an FR-positive L929 tumor model. FA–PEG_{4K}–PAMAM–Gd showed a high affinity for the surface of the L929 cell lines with high

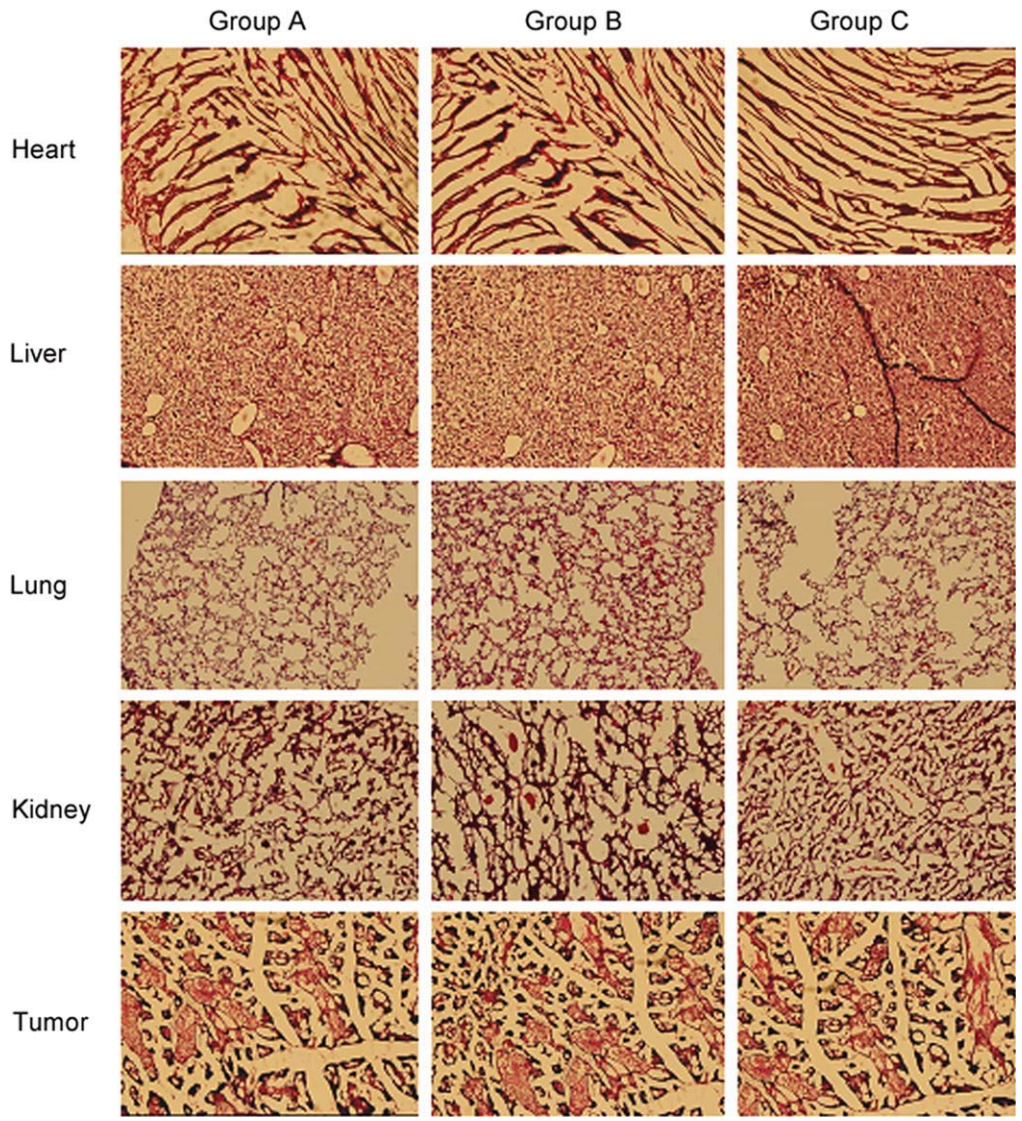

Figure 9 Toxicity assay of FA–PEG_{4K}–PAMAM–Gd in the liver, heart, tumor, kidney, and lungs of mice. Biocompatibility is indicated by a comparison of the normal organs preinjection (group A) with organs 3 days postinjection (group B) and 3 months postinjection (group C). [Color figure can be viewed in the online issue, which is available at wileyonlinelibraray.com.]

density, as shown in Figure 8(b). FA–PEG_{4K}–PAMAM–Gd remained on the surface of the L929 cells even after they were cultured for 3 h. A competitive assay provided proof that the affinity was indeed via the FR. FA–PEG_{4K}–PAMAM–Gd appeared to be clearly very effective for FR targeting.

In vivo toxicity evaluation

To determine the toxicity of FA–PEG_{4K}–PAMAM–Gd, potential pulmonary, renal, liver, cordis, or cancer tumor damages were examined within the three groups of mice. All of the mice showed no adverse effects after injection with this contrast agent. The shape and structure of myocardium tissue were normal and densely arranged (groups B and C) without apoptosis. The destruction of cells even after continuous injection for 3 months, compared with the normal microstructure of these organs (group A), are shown in Figure 9. There were no differences between group B (3 days after injection) and group C (3 months after injection) after continuous injection of FA–PEG_{4K}–PAMAM–Gd. FA–PEG_{4K}–PAMAM–Gd also did not exhibit chronic toxicity to the heart at a dosage of 0.1 mmol/kg. The same results were obtained from the lung, liver, kidney, and tumors (Fig. 9). All of these results indicate that FA–PEG_{4K}–PAMAM–Gd did not exhibit chronic toxicity at a dose of 0.1 mmol/kg for mice; this further implies good biocompatibility and potential clinical applications.

CONCLUSIONS

FA–PEG–PAMAM–Gd contrast agents with a PAMAM core displayed a higher signal enhancement and lower concentration detection limits. The macromolecular contrast agent of FA–PEG_{4K}–PAMAM–Gd did not exhibit toxicity at the dosages that we used. TEM images indicated that FA–PEG_{4K}–PAMAM–Gd could target KB and L929 cell lines with high affinity. The distribution of FA–PEG_{4K}–PAMAM–Gd in tumors (>240 min) was longer than that of the low-M_w contrast agent DTPA–Gd. Furthermore, tumors 3 mm in size (diameter) showed good delineation after the injection of FA–PEG_{4K}–PAMAM–Gd. These results indicate that FA–PEG_{4K}–PAMAM–Gd is a promising contrast agent for the early diagnosis of cancer. However, the drawback of the increased PDI of FA–PEG–PAMAM–Gd should be overcome to improve their biocompatibility.

The authors thank Weiwei Men from Shanghai Key Laboratory of FMRI for his assistance of MRI measurement.

References

1. Lauffer, R. E. Chem Rev 1987, 87, 901.
2. Weissleder, R.; Mahmood, U. Radiology 2001, 219, 316.
3. Edelman, R. R.; Warach, S. N Engl J Med 1993, 328, 708.
4. Martin, G.; Pomper, M. D. Acad Radiol 2001, 8, 1141.
5. Aime, S.; Barge, A.; Cabella, C.; Crich, S. G.; Gianolio, E. Curr Pharm Biotechnol 2004, 5, 509.
6. Caravan, P.; Ellison, J. J.; McMurry, T. J.; Lauffer, R. B. Chem Rev 1999, 99, 2293.
7. Mecke, A.; Uppuluri, S.; Sassanella, T. M.; Lee, D. K.; Ramamoorthy, A.; Baker, J. R., Jr.; Orr, B. G.; Banaszak Holl, M. M. Chem Phys Lipids 2004, 132, 3.
8. Mecke, A.; Lee, D. K.; Ramamoorthy, A.; Orr, B. G.; Banaszak Holl, M. M. Langmuir 2005, 21, 8588.
9. Wiener, E. C.; Brechbiel, M. W.; Brothers, H.; Magin, R. L.; Gansow, O. A.; Tomalia, D. A.; Lauterbur, P. C. Magn Reson Med 1994, 31, 1.
10. Fischer, M.; Vögtle, F. Angew Chem Int Ed 1999, 38, 885.
11. Stiriba, S. E.; Frey, H.; Haag, R. Angew Chem Int Ed 2002, 41, 1329.
12. Smith, P. E. S.; Brender, J. R.; Dürr, U. H. N.; Xu, J. D.; Mullen, D. G.; Banaszak Holl, M. M.; Ramamoorthy, A. J Am Chem Soc 2010, 132, 8087.
13. Kobayashi, H.; Brechbiel, M. W. Adv Drug Delivery Rev 2005, 57, 2271.
14. Kono, K.; Kojima, C.; Hayashi, N.; Nishisaka, E.; Kiura, K.; Watarai, S.; Harada, A. Biomaterials 2008, 29, 1664.
15. Calabretta, M. K.; Kumar, A.; McDermott, A. M.; Cai, C. Z. Biomacromolecules 2007, 8, 1807.
16. Wang, W.; Xiong, W.; Wan, J. L.; Sun, X. H.; Xu, H. B.; Yang, X. L. Nanotechnology 2009, 20, 105103.
17. Labieniec, M.; Watala, C. Cent Eur J Biol 2009, 4, 434.
18. Wu, P. C.; Su, C. H.; Cheng, F. Y.; Weng, J. C.; Chen, J. H.; Tsai, T. L.; Yeh, C. S.; Su, W. C.; Hwu, J. R.; Tzeng, Y.; Shieh, D. B. Bioconjugate Chem 2008, 19, 1972.
19. Bueno, R.; Appasani, K.; Mercer, H.; Lester, S.; Sugarbaker, D. Thorac J Cardiovasc Surg 2001, 121, 225.
20. Reddy, J. A.; Low, P. S. Crit Rev Ther Drug Carrier Syst 1998, 15, 587.
21. Lu, Y.; Low, P. S. Cancer Immunol Immunother 2002, 51, 153.
22. Wiener, E. C.; Konda, S.; Shadron, A.; Brechbiel, M.; Gansow, O. Invest Radiol 1997, 32, 748.
23. Konda, S. D.; Aref, M.; Wang, S.; Brechbiel, M.; Wiener, E. C. Magn Reson Mater Phys Biol Med 2001, 12, 104.
24. Zalipsky, S.; Gilon, C.; Zilkha, A. Eur Polym J 1983, 19, 1177.
25. Langereis, S.; de Lussanet, Q. G.; van Genderen, M. H. P.; Meijer, E. W.; Beets-Tan, R. G. H.; Griffioen, A. W.; van Engelshoven, J. M. A.; Backes, W. H. NMR Biomed 2006, 19, 133.
26. Chandrasekar, D.; Sistla, R.; Ahmad, F. J.; Khar, R. K.; Diwan, P. V. J Biomed Mater Res Part A 2006, 82, 92.
27. Zhang, W. L.; Li, N.; Huang, J.; Yu, J. H.; Wang, D. X.; Li, Y. P.; Liu, S. Y. J Appl Polym Sci 2010, 118, 1805.
28. Singh, P.; Gupta, U.; Asthana, A.; Jain, N. K. Bioconjugate Chem 2008, 19, 2239.
29. Barrett, T.; Kobayashi, H.; Brechbiel, M.; Choyke, P. L. Eur J Radiology 2006, 60, 353.